Advances in understanding mobilization processes of trace metals in marine sediments

Chunyang Zhou[a], Yue Gao[a*], Camille Gaulier[a,b], Mingyue Luo[a], Xiaohan Zhang[a], Arne Bratkic[a], William Davison[c], Willy Baeyens[a]

[a] Analytical, Environmental and Geo-Chemistry department (AMGC), Vrije Universiteit Brussel (VUB), Pleinlaan 2, 1050 Brussels, Belgium

[b] LASIR CNRS UMR 8516, Universite de Lille, Cite Scientifique, 59655 Villeneuve d'Ascq Cedex, France

[c] Lancaster Environment Centre, Lancaster University, Lancaster LA1 4YQ, United Kingdom

*corresponding author: Yue GAO, email: yue.gao@vub.be

10 TOC

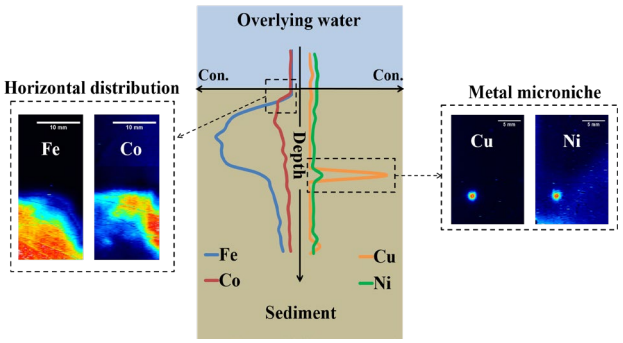
Overlying water
Horizontal distribution
Con.
Con.
Metal microniche
Fe
Co
Depth
Cu
Ni
Fe
Co
Cu
Ni
Sediment

11

ABSTRACT

Different mobilization mechanisms control the metal distribution in surface sediments of the Belgium coastal zone (BCZ) and the anoxic Gotland basin (GB). This mobilization was studied using DGT (Diffusive Gradients in Thin-films): vertical 1D profiles of Cd, Co, Cu, Fe, Mn, Ni, Pb, and Zn were measured at 5 mm intervals, while 2D high-resolution (100 μm) images of smaller zones of the sediment profile were obtained on separate DGT probes. Removal of dissolved Cd, Cu, and Pb in BCZ sediments caused steep vertical gradients at the sediment water interface that were well replicated in 1D profiles and 2D images. While 1D profiles showed apparent coincident maxima of Co, Mn, and Fe, 2D images revealed mutually exclusive Co and Fe mobilization. Correlation analysis supported this observation and showed a consistent linkage between Co and Mn. Sharp maxima of some metals in the vertical 1D profiles of GB sediment were attributed to localized mobilization in microniches. Examination of a ~1 mm diameter Cu and Ni maximum in 2D, defined by ~300 data points, showed that the metals were supplied from localized decomposition of reactive organic material, rather than release from reductively dissolving Fe or Mn oxides, and that they were removed as their sulfides.

Key words: high resolution, two-dimensional imaging, trace metal mobilization, microniche, sediment water interface, Diffusive Gradients in Thin-films

INTRODUCTION

The decomposition of organic matter and associated dissolution of Fe/Mn hydroxides can facilitate the remobilization of trace metals from sediment to porewater and in some cases to the water column.[1,2] These processes have traditionally been studied by (1) collecting sediment cores, (2) slicing the sediment at 1 cm or more vertical intervals, which typically represents 20-80 mL of sediment,[3] and (3) analyzing both solid and liquid phases. Our knowledge and modeling of early diagenesis is based on such measurements. Smaller scale sediment processes have been explored by making measurements at a finer scale of μm to mm,[2,4] and in a few cases two dimensional (2D) images of solutes have been obtained.[5,6] These new developments showed that remobilization processes may be occurring at discrete, small-scale locations (microniches) at various depths within surface sediments, indicating that diagenesis should not be solely considered as processes occurring sequentially with depth.

Microelectrodes have played an important role in appreciating small-scale variations of many solutes, including oxygen, nitrogen species, sulfide, and iron and manganese,[7,8] while planar optodes (PO) have provided high resolution oxygen and pH information in two dimensions.[9] Two dimensional and high resolution (2D-HR) distributions of various trace metals have been obtained using the DGT (Diffusive Gradients in Thin-films) technique, consisting of a diffusive gel backed by a binding gel.[6,10] DGT determines localized fluxes of metals that can be interpreted as dissolved concentrations.[11] For analysis of trace metals subsequent to deployment, the gel binding the analyte is either sliced into small strips (e.g., 5 mm intervals), providing 1D profiles, or scanned directly by laser ablation coupled with ICP-MS (LA-ICP-MS) to obtain 2D images. Grey scale 2D images of dissolved sulfide that can be interpreted as concentrations can also be obtained by using a silver iodide (AgI) binding gel.[6] A resolution of 100 μm × 100 μm (or even

54 finer), determined by the laser beam diameter or the dpi of a scanner, can be achieved by both 2D
55 imaging methods.[12] It is fine enough to observe microniches with a diameter principally varying
56 from a few tens of microns up to the millimeter scale.[13]

57 The formation of mobilization microniches is normally attributed to local decay of organic
58 substrates such as algal aggregates[14] and faecal pellets[15] by microorganisms,[16] where available
59 oxidants (nitrate, Fe and Mn oxides, and sulfate) are quickly depleted and the associated trace
60 metals are subsequently released. Other mechanisms that can create microniches are those linked
61 to acidification of the porewater and dissolution of acid sensitive metal sulfides or carbonates,[17]
62 or to oxidation of reduced metal solids. For example iron sulfides can be oxidized microbially
63 with stronger oxidants than sulfate (Fe/Mn oxides or nitrate) as electron acceptor.[18] Elevated
64 concentrations of trace metals within microniches can thus be observed, which can be several-
65 folds higher than that in bulk sediment,[6] resulting in accelerated trace metal recycling rates. A
66 limited number of other studies on trace metal mobilization in microniches using DGT combined
67 with LA-ICP-MS have been reported. In experimentally manipulated systems, without
68 complementary larger scale measurements, Stahl et al.[5] demonstrated localized elevated
69 mobilization of Ni, Cu, and Pb close to a burrow wall in a sediment mesocosm, and Lehto et al.[19]
70 showed that microniches can make a significant contribution to organic matter turnover at the
71 sediment-water interface (SWI) and promote a high degree of variability in the cycling of
72 associated compounds and trace metals in surface sediments. Direct measurements in unmodified
73 sediment cores have focused on the simultaneous remobilization of dissolved sulfide and trace
74 metals.[6,20] In those studies, attention was primarily paid to method development and optimization
75 to detect the occurrence of microniches. The underlying mobilization mechanisms, explaining
76 which sediment processes are linked to the increased metal and/or sulfide concentrations,

77 remained unclear. Moreover, detailed comparison of small-scale trace metal mobilization
78 observed by 2D images and 1D profiles and the information that can be extracted from each of
79 these results, has scarcely been made.

80 In this study, we selected two contrasting environments, namely the Belgian coastal zone (BCZ,
81 in the North Sea) and the Gotland basin (GB, in the Baltic Sea), where the bottom waters are oxic
82 and anoxic respectively. This difference in redox conditions induces distinct diagenetic processes
83 in the sediment and thus allows investigation of the underlying mobilization mechanisms in
84 contrasting environments. We use a novel research approach to measure trace metals in
85 undisturbed, natural sediment cores, whereby 1D profiles (5 mm resolution obtained by slicing
86 DGT gels) were complemented with 2D-HR imaging (100 μm resolution obtained by DGT and
87 LA-ICP-MS). With the 1D profiles, which are easier to obtain over larger spatial distances, we
88 search for coincident peaks of trace metals and sulfide. The 2D images are then used to detect
89 small, localized mobilization areas in the same sediment zone where the 1D peaks were found,
90 and to further investigate on a detailed spatial scale the local diagenetic processes, enabling
91 identification of mobilization mechanisms.

92 **MATERIALS AND METHODS**

93 **Sampling sites and collection of sediment cores**. There were a total of 5 sampling stations in
94 the two study regions (BCZ and GB) (Figure S1): Station 130, located in BCZ; Stations 8, 6, 14,
95 and 16, located in GB. Detailed information on the sampling stations are reported in the
96 supporting information (SI). Two sediment cores with an overlying water layer of ~4 cm were
97 collected at station 130 in October 2017. They were immediately transported back to the
98 laboratory and placed in a tank filled with seawater collected at the same station. An aerating
99 device was installed in the tank to maintain an adequate oxygen level, corresponding to that at

station 130, in the overlying water. Similarly, two sediment cores with an overlying water layer of ~4 cm were collected at stations 8, 6, 14, and 16 in June 2018. As the bottom water at these four stations was anoxic (< 0.3 mg L^{-1} of oxygen), the sediment cores were sealed with parafilm immediately after collection to avoid oxygen ingress and placed in a tank filled with flowing seawater to keep the ambient temperature constant on board. General features of the sediments in BCZ and GB (salinity, pH, and sediment layer structure) are reported in the SI.

Preparation of DGT probes. A DGT probe is a rectangular, plastic moulding enclosing a binding gel layer, covered sequentially by a diffusive gel and a protecting filter membrane, and closed by a plastic front plate, with a window of 150 × 18 mm that exposed the filter membrane to the sediment. Two different types of DGT probes were used in this study; a ground Chelex-100 (GCH) probe for metals and a silver iodide (AgI) probe for dissolved sulfide. GCH resin was made according to Zhou et al.[21], with a minor modification to improve the efficiency of the grinding process and consequently obtain a smaller bead size of resin powder. Two grams of the ground resin were soaked overnight in 40 mL 1 M nitric acid in a 50 mL centrifuge tube. The cleaned resin was then washed thoroughly with MilliQ (MQ) water several times to remove the residual H^+. The cleaned resin was converted to the sodium form necessary for DGT performance (details are reported in the SI) by adding 0.5 M NaOH to reach pH 11 and then washed thoroughly with MQ water to remove the residual OH^-. Blank values of metals on a GCH binding gel disc were determined by eluting with 1 mL 1M nitric acid (see Table S1). AgI gel was made according to Gao et al.[6]. Standard polyacrylamide hydrogels, 0.8 mm thick, cross-linked with an agarose derivative were used for all diffusive gels. Filters were hydrophilic PVDF (polyvinylidene fluoride) membranes from Durapore®. Diffusive gel preparation, filter cleaning, and DGT probe assembly followed published procedures.[6]

Prior to deployment, DGT probes were deoxygenated overnight in 0.1 M NaCl solution continuously bubbled with N_2 gas.

DGT probes deployment and retrieval. DGT probes were vertically inserted into the sediment cores with minimum disturbance, leaving around 2 centimeters of the window area of the probe above the SWI. For station 130, GCH and AgI DGT probes were arranged back-to-back and inserted into a sediment core. A duplicate deployment was made in a separate core collected from the same station. After 10 hours deployment, the four probes were simultaneously retrieved and the exposure window was thoroughly rinsed several times with MQ water. For each GB station 8, 6, 14, and 16, one GCH and one AgI DGT probe were inserted into separate sediment cores. A deployment time of 4 hours was adopted for the AgI probes to avoid saturation by the high sulfide concentrations. Deployment time of 20 hours was used for the GCH probes. After deployment, probes were retrieved and rinsed thoroughly. Binding gels were peeled from the probes prior to treatment.

Sample treatment and analysis. *GCH binding gels treatment and analysis*. For determination of 1D metal profiles, the GCH binding gels from stations 8, 6, and 14 in GB and station 130 in BCZ were sliced vertically at 5 mm intervals. Each slice was eluted with 1mL 1M HNO_3 for 24 hours before ICP-MS measurement of the diluted eluent.

For determination of 2D metal images, the GCH binding gels from station 16 in GB and station 130 in BCZ were placed on a clean PVDF filter prior to the drying procedure as described previously.[6,21] Briefly, the binding gel and filter were dried together at 60°C for 24 hours using a gel drier (Model 583, Bio-Rad) connected to a vacuum pump. Afterwards, the dried binding gel was cut to a suitable size and mounted on a micro-slide by double-sided tape before LA-ICP-MS analysis. Details of the LA-ICP-MS settings are shown in Table S2.

Treatment of AgI binding gels and analysis by computer imaging densitometry (CID). The color change of the gels from pale yellow to various shades of grey is due to the formation of AgS. A greyscale image, obtained using a flat-bed scanner (HP 3100), was processed by Fiji software (Fiji is an open source image processing package based on ImageJ) and the concentration of dissolved sulfide was calculated using the calibration curve plotted in Figure S3. Details relating to the calibration curve are reported in the SI. 1D depth profiles of dissolved sulfide were obtained by averaging 2D images over the horizontal dimension.

The Person method was used to evaluate the significance of correlation between different metals at significance levels of 0.05 and 0.01 (Sigmaplot 14.0, Systat Software Inc.). QA/QC is reported in the SI.

RESULTS

1D profiles of dissolved metals and sulfide in the sediment at station 130 (BCZ). The 1D profiles of metals in the sediment at station 130 (BCZ) have two distinct patterns (Figure S4). Cd, Pb, Ni, Cu, and Zn all had higher concentrations in the overlying water that declined steeply across the SWI and then remained at a much lower level down to the bottom of the DGT probe. There were some localized maxima below the SWI. Cu increased up to 53 nM at -9 cm, which was 35 times higher than the background concentration of 1.5 nM (averaged value of three concentration points either side of the observed metal maximum). This Cu maximum was coincident with a small Pb peak of 2.4 nM, which was 5 times higher than the background concentration. Three dimensional modeling has shown that coincident sharp peaks of several metals in a DGT profile are characteristic of mobilization from localized microniches.[22] This suggests that there is likely a microniche of elevated Cu and Pb mobilization. Zn increased to 400

nM at -7 cm, which was 2.7 times higher than the background value of 150 nM, which would imply a microniche where only one metal is mobilized.

The sediment profiles of Fe, Mn, and Co were distinctly different from those described above (Figure S4). Their concentrations in the overlying water were close to zero, but increased markedly below the SWI. They reached 90 μM for Fe and 40 μM for Mn around -3 cm depth, remained constant for another 2 cm and decreased sharply at greater depth. Co also peaked in concentration (20 nM) at around -3 cm, but the peak was narrower than that for Fe and Mn, due to a progressively decline from -3 cm depth. The decline with depth of Fe, Mn, and Co most likely reflects precipitation of their sulfides as the concentration of dissolved sulfide generally increased from -7 cm to the bottom of the probe (Figure S4). A small peak of dissolved sulfide was observed at around -1 cm depth below the SWI where the concentrations of Fe, Mn, and Co were also high. Such simultaneous occurrence of metals and sulfide has been attributed to the degradation of reactive organic material that is abundantly present and the concurrent reduction of a number of oxidants, including sulfate.[20,23]

2D-HR images of dissolved metals and sulfide at the SWI of station 130 (BCZ). The SWI (1 to -2 cm) was selected for more detailed analysis to investigate further the contrasting mobilization patterns of the two groups of elements. Consistent with 1D profiles, Cd, Cu, and Pb were more abundant in the overlying water, decreasing markedly across the SWI, while Fe, Mn, and Co were more concentrated below the SWI (Figure 1). Images of Ni and Zn are not shown because their results were close to the detection limit of LA-ICP-MS, as previously reported.[21] Considering the data are from deployments in separate cores, the horizontally averaged concentrations were similar to those observed from the 1D profiles and the location of the main gradient change coincided remarkably well (Figure 2). However, the 2D images showed that

there were distinct horizontal gradients, not detectable from 1D profiles. Above the SWI, Pb and Cd were more elevated at the left side of the image. Below the SWI, Fe was elevated at the left side of the image while Co was more concentrated at the right side. Mn was more homogeneously distributed compared to Fe and Co. Consistent with the small peak below the SWI found in the 1D profile, the 2D image showed that dissolved sulfide was elevated in this region, but its horizontal distribution is not uniform: the zone of sulfide mobilization being closer to the SWI at the centre of the 2D image. The detail provided by the 2D image suggests that the zones of Fe and Co mobilization occur at different locations. Not surprisingly, the greatest differences in horizontally averaged concentrations from those of the 1D profiles are for Fe and Co, the two metals with the greatest horizontal variation in their 2D images (Figures 1 and 2).

1D profiles of dissolved metals and sulfide in sediments at stations 8, 6, and 14 (GB). The 1D profiles of dissolved metals and sulfide in the sediment at station 8 (GB) are shown in Figure S5. Cd showed a maximum at -5 cm, with the concentration reaching 1.0 nM, while a narrower maximum of 6.8 nM was found at the same depth for Cu. A coincident peak of Pb, Cu, and Fe was found at -2 cm, with maximum concentrations of 0.4 nM, 6.5 nM, and 0.8 μM respectively. Concentrations of Fe and Co were generally much lower in the porewaters of station 8 compared to those of station 130. The maximum concentration of Fe, equal to 0.8 μM, appearing at -2 cm, was 110 times lower than the peak concentration of 90 μM at station 130. Similarly, a 14 times difference was found for Co. Formation of metal sulfides due to the high level of sulfide (up to 90 μM) at station 8 is most likely responsible for this huge difference (Figure S5). Mn, which is more likely to form carbonates than sulfides,[24] increased progressively with depth to reach a concentration of 7 μM. Manganese-calcium-carbonate-phosphate minerals have been observed in GB sediments.[25,26] Under anoxic conditions this solid phase acts as a source for Mn and

phosphate in the porewater and is responsible for the observed similar depth profiles of Mn and phosphate concentrations in GB porewaters.[27]

With the exception of Mn, which consistently increased with depth, irregular metal mobilization patterns were observed in the sediments at stations 6 and 14 (Figures S6 and S7). Although there was no clear trend with depth for Ni and Cu, there were two distinct, coincident maxima at -6 cm and -11 cm in the core from station 6. Similarly, a peak for Fe, Mn, Ni, Cu, and Zn was observed at -2 cm depth at station 14. Summarizing, three potential microniches with elevated mobilization of various elements were observed: Cu and Ni at station 6 (at -6 and -11 cm depths), Pb, Cu, and Fe at station 8 (at -2 cm depth), and Fe, Mn, Ni, Cu, and Zn at station 14 (at -2 cm depth).

2D-HR images of dissolved metals and sulfide in sub-surface sediment at station 16 (GB). The mobilization of metals and sulfide in the sub-surface zone (-8.5 cm to -10.5 cm) were further investigated by 2D-HR imaging in the sediment at station 16 (GB) (Figure 3). Cd and Pb concentrations stayed low in this zone (below 1.5 nM for Cd and 3 nM for Pb) without clear gradients. Two spheroidal microniches (diameter around 1 mm) were observed for Cu and Ni at exactly the same location indicating that they were mobilized simultaneously with maximum concentrations up to 350 and 150 nM respectively. A zone of elevated Fe concentrations covering an area of around 1 cm^2 occurred between -9.5 and -10.5 cm depth. The maximum concentration of 20 μM in this zone was much higher than the concentration of Fe (below 1 μM) in the sediments at other GB stations. The maximum concentration (35 μM) of Mn was consistent with the findings at other GB stations. Although Mn was slightly elevated in the lateral centre of the image, overall, unlike Fe, it declined progressively with depth. Sulfide was more enriched in the upper- and lower- left parts of the image.

DISCUSSION

237 The traditional way to study the mobilization of metals and sulfide in sediments is to slice the
238 solid phase at a vertical resolution of 1 to 5 cm followed by porewater extraction.[28] The technique
239 of DGT with manual gel cutting can achieve a vertical resolution as low as 0.1 cm.[29] This
240 improvement in resolution has been well documented and discussed.[4,28,30] However, because the
241 volume of sediment contributing to each DGT data point, of typically 0.02-0.1 mL, is much
242 smaller than in conventional sampling, concentration-depth profiles can appear to be noisy,
243 especially if there are near spherical microniches of mobilization occurring at the mm scale.
244 Consequently, it can be more difficult to assess the overall mobilization trends.[2,30] One way of
245 overcoming these deficiencies, is to make measurements on a finer scale in two dimensions so
246 that highly localized concentration maxima are accurately characterised by a set of data points
247 rather than a few or even a single data point in one dimension. This goal has been achieved by
248 measuring DGT binding gels in two dimensions at typically 50 to 100 μm spatial resolution,
249 using LA-ICP-MS for determination of metals and computer imaging densitometry for sulfide
250 determination.[6,21] With this higher resolution, smoother transitions can be observed between
251 lower and higher concentration zones, allowing microniches of mobilization at the mm scale to
252 be fully resolved. The drawback is that collecting such data is expensive and time consuming,
253 placing limits on the number and size of binding gels that can be analysed. This work investigates
254 how well using DGT with vertical slicing at the 5 mm scale, allied to selective samples of much
255 finer scale 2D imaging, can complement each other to advance understanding of sediment
256 processes.

257 **Understanding the horizontal gradients of metals and sulfide in the sediment**. The 1D profile
258 of metals in our study was generated by manually gel cutting at 5 mm intervals. Thus every
259 single point in the 1D profile represents the average concentration of a 0.5 × 1.8 cm^2 (length ×

width) rectangle piece of binding gel. Such a rectangle contains more than 8000 data points in our 2D-HR image. To illustrate how the detailed information obtained from a 2D-HR image compares with information from a 1D profile, two zones in the sediment at station 130 (Figures 1 and 4A), where metals were strongly mobilized, were selected. Zone 1 (0.25 to -0.25 cm of depth) in the 2D image corresponds to the concentration point at 0 cm in the 1D profile, while zone 2 (-1.25 to -1.75 cm of depth) in the 2D image corresponds to the point at -1.5 cm in the 1D profile. Statistical analysis of the distribution of concentrations of Cd, Cu, and Pb in zone 1, and of Fe, Mn, and Co in zone 2 of the 2D image showed that the concentrations of each metal were normally distributed, as demonstrated by the small difference observed between mean and median values (Figure 4B). However, due to the considerable concentration gradients within each zone, there was a substantial range in concentrations. Co had the largest maximum/minimum ratio of 4.8 while for Mn, Cd, Cu, Pb, and Fe it was 1.7, 2.3, 2.4, 2.7, and 4.3 respectively. Higher ratios reflect steeper concentration gradients that drive diffusional fluxes of the metal in and out of the zone. None of this information can be accessed from the single data point of the 1D profile.

Our study provides strong evidence that Co was not co-mobilized with Fe (Figure 1). The 2D image shows that the zones of mobilization of Fe and Co were virtually mutually exclusive. This is illustrated more conventionally by Figure 4C, which shows the horizontal gradients of Fe, Mn, and Co in zone 2. Fe declined steeply at around 1 cm distance from the left edge of the 2D image, whereas the steep increase in Co started at this distance. There was a consistent, but modest rise in Mn from left to right. Correlation analysis between these metals (Fe, Mn, and Co) was performed using data from different sources: 1D vertical profiles (1D, 1 to -2 cm depth, shown in Figures 2 and S4), 1D vertical profiles from horizontally averaged 2D images (1DV2D, 1 to -2 cm depth, shown in Figure 2), 1D horizontal transects from vertically averaged 2D images within

283 zone 2 (1DH2D, shown in Figure 4C) and the entire 2D images (E2D, shown in Figure 1). There
284 were significant positive correlations ($R^2 > 0.8$, $p < 0.01$) between these metals for 1D and
285 1DV2D profiles (Table 1). However, negative correlations were found for Fe/Mn ($R^2 = -0.59$, $p <$
286 0.01) and Fe/Co ($R^2 = -0.97$, $p < 0.01$) for the horizontal transect (1DH2D). These apparently
287 contradictory results illustrate the danger in relying solely on information from 1D vertical
288 profiles where the sampling technique incorporates horizontal averaging. Consideration of data
289 for the entire 2D image automatically includes both vertical and horizontal information, but any
290 correlation will be weakened by the presence of regions without gradients. The best correlation
291 was for Mn and Co ($R^2 = 0.68$, $p < 0.01$), but Mn and Fe also correlated significantly ($R^2 = 0.54$,
292 $p < 0.01$). There was no significant relationship between Fe and Co ($R^2 = 0.40$, $p > 0.05$).
293 Whichever data source was used, the relationship between Mn and Co was significant (Table 1).

294 Coincident maxima of Co and Mn observed in vertical 1D profiles have been previously
295 interpreted as evidence for their co-mobilization from reductive dissolution of oxides.[4,31]
296 Although similar concentration maxima for Co and Fe were observed in a marine sediment, they
297 were thought to be due to removal of Fe and Co as their sulfides rather than Co being released
298 during reduction of authigenic Fe oxides.[32] Attribution of Co mobilization to either Fe or Mn
299 processes would not have been possible from our 1D measurements, but the 2D image securely
300 demonstrates there is no relationship with Fe and a strong one with Mn. The behavior of Mn and
301 Co in the marine environment is strongly linked to each other since Co(II) is oxidized to Co(III)
302 in the same Eh-pH space where Mn(II) oxidation occurs,[33] accounting for the oxidation of Co(II)
303 and adsorption of Co(III) to precipitated Mn(III, IV) oxides.[34] Iron(II) is oxidized to Fe(III) at a
304 lower redox potential than Co(II) and Mn(II) at marine pH (7-8) and is less associated with Co.
305 Therefore, Co enters sediment mainly associated with Mn hydroxides and is released to

306 porewater concurrently with Mn. Cable bacteria are known to be prevalent in the sediment at
307 station 130 (BCZ).[17,35] From the modeling of the effects of cable bacteria on chemical profiles,
308 van der Velde et al.[17] concluded that, due to the lowered pH that is similar to our observation
309 (Figure S2), Mn(II) was largely supplied from dissolution of $Ca(Mn)_xCO_3$ in addition to
310 dissolution of Mn hydroxides. Although Fe(II) was partly supplied from dissolution of FeS,
311 reductive dissolution of iron oxides was still dominant. The different remobilization processes of
312 Fe and Mn are likely the explanation for their different distributions in our 2D image which
313 provides the first direct evidence for their mechanistic decoupling.

314 There were marked horizontal gradients of sulfide in zone 2 (Figure S8). As the sulfide image
315 was obtained from a different deployed probe to the trace metals precise locational comparison is
316 not justified, but it further illustrates the steep horizontal gradients of reduced species in this
317 sediment.

318 **Characterisation of trace metal microniches in sediment**. The 1D profiles in the GB sediments
319 (Figures S5, S6, and S7) suggest the potential existence of microniches of trace metal
320 mobilization, as certain metals peak at the same depth. Single point elevations do not allow
321 characterization of the shape, size or nature of a microniche. However, a well-defined, circular
322 elevation of Cu and Ni was observed in a 2D-HR image from GB sediment (Figure 3). This
323 mobilization microniche, which had a diameter of ~1 mm and was defined by around 300
324 individual data points, would have appeared as a single point in our 1D profiles. No other metals
325 were elevated at the same location.

326 Previous studies have suggested that two distinct processes may be responsible for such localized
327 mobilization. Using 2D DGT in a marine sediment incubation experiment, Lehto et al.[19] observed
328 two sub-surface microniches (around 1.5 and 2.5 mm^2 respectively) where Co, Ni, and Zn were

329 substantially mobilized. They were attributed to release during the dissolution of Fe and Mn
330 oxides, as there was coincidental elevation of Fe and Mn. Similarly, Motelica-Heino et al.[20]
331 observed elevated Co, Ni, Cu, Fe, and Mn, along with sulfide, in a ~4 mm diameter microniche
332 of a freshwater sediment. While Fones et al.[2] in their 1D DGT study of North Atlantic sediments
333 observed coincident peaks of Ni, Cu, Cd, and Zn with Fe and particularly Mn, they considered
334 there was more evidence in favor of the trace metals being released from organic material.
335 Tankere-Muller et al.[4] found the simultaneous release of Cu and Cd near to the surface of the
336 sediment of a marine microcosm. As this was above the mobilization zone of Fe and Mn, their
337 release was attributed to the degradation of organic matter as it oxidized at the sediment surface.
338 In another mesocosm study, Stahl et al.[5] observed localized co-mobilization of Cu and Ni close to
339 the wall of an artificial burrow. The high O_2 levels in the burrow excluded release from reductive
340 dissolution of oxides and favored release from rapidly oxidising organic matter. More generally,
341 the transport of Cu and Ni in marine systems is predominantly controlled by biological uptake
342 and adsorption on organic matter rather than on Fe oxides.[36,37] Hence, Cu and Ni have been used
343 as proxies for the organic carbon sinking flux.[38,39] We examine which of these two mechanisms,
344 release from decomposing organic material or during reductive dissolution of oxides, can account
345 for the observed Ni and Cu microniche.

346 Figure 5 shows the metal concentrations along a single laser ablation line that transects the Cu
347 and Ni microniche. A prominent peak of Cu and Ni was observed at the same location. Fe
348 slightly increased across the transect with no indication of a peak, while Mn remained constant
349 throughout. The absence of coincident features in the Fe or Mn transects favours localized
350 degradation of organic matter as the source of Cu and Ni to the porewater, but examination of

metal ratios in metal oxides and organic material, as well as consideration of the role of sulfide, provide a more quantitative perspective.

Tessier and co-workers[40,41] obtained authigenic phases of iron deposited in situ on plastic plates inserted into sediments. The metal ratios (0.81 mmol Cu / mol of Fe, 0.63 mmol Ni / mol of Fe) they found were comparable to the ratios reported in other studies of freshly formed oxides.[42–44] These ratios allow estimation of the concentration of Cu and Ni that can be potentially generated from the reductive dissolution of iron oxides. If the entire Fe concentration within the microniche zone of 10 μM is attributed to localized reductive dissolution, corresponding concentrations of Cu and Ni that would be simultaneously released are 8.1 nM and 6.3 nM respectively (Figure 5). These values are much lower than the observed peak concentrations of 250 nM Cu and 100 nM Ni. As there is no apparent concentration increase of Mn within the microniche, the co-release of Cu and Ni from the dissolution of Mn oxides is less likely. Furthermore, in anoxic GB sediments, Mn carbonates are the dominant form of Mn in the sediment solid phase, which account for over 50% (up to 90% for deep stations) of total Mn, while the percentage of Mn oxides is generally less than 5%.[27] The association of Cu and Ni with Mn carbonates is weak,[45,46] suggesting that their release from the dissolution of Mn carbonates is an unlikely source.

Natural phytoplankton species are a major source of reactive organic matter deposited on the sediment surface, but the trace metal to organic carbon ratios in phytoplankton varies widely among species and marine areas.[47,48] The most common species that is well-developed in summer time at the GB of the Baltic Sea is nitrogen-fixing cyanobacteria,[49] in which the ratios of metal/carbon (mmol/mol) are 7.8 for Cu and 1.8 for Ni.[48] With these ratios, the organic carbon concentration, necessary to comply with the peak concentrations of Cu (250 nM) and Ni (100 nM), is between 30 and 50 μM of carbon. As the average HCO_3^- concentration of porewater in

374 GB surface sediment is almost 2800 μM,[50,51] degradation of 50 μM of organic carbon will
375 increase the HCO_3^- concentration by less than 2%. Given the uncertainty of solely applying the
376 metal/carbon ratio, the metal/nitrogen and metal/phosphorus ratios were also calculated to
377 constrain the uncertainty. For the same cyanobacteria species with Cu/C and Ni/C ratios of 7.8
378 and 1.8, the ratios of Cu/N and Ni/N are 48 and 11 (mmol/mol) respectively, and those of Cu/P
379 and Ni/P are 1.0 and 0.24 (mol/mol) respectively. This means that 5 to 10 μM of NH_4^+ and 0.25
380 to 0.42 μM of HPO_4^{2-} would be co-released during organic carbon degradation to comply with
381 the peak concentrations of Cu and Ni. Given the concentrations of NH_4^+ and HPO_4^{2-} in GB
382 surface sediment are generally higher than 75 and 30 μM respectively,[27,50] the co-released NH_4^+
383 and HPO_4^{2-} will have no influence on their porewater concentrations. These calculations as well
384 as the findings of Ingri et al.[52], that the input of Cu and Ni to Baltic Sea sediments is dominated
385 by the deposition of organic particles from the water column, further support the idea that the
386 origin of the Cu and Ni microniche is from localized decomposition of organic matter.

387 Dynamic, three-dimensional modeling of process in microniches has suggested that localized
388 formation of metal sulfides can be an important sediment process.[13] Mineral saturation indices
389 (SI) for Fe, Mn, Cu, and Ni sulfides inside and outside the microniche were calculated using
390 Visual Minteq. Results are shown in Table S4 and detailed discussion is available in the SI. Our
391 results are in agreement with the finding of Stockdale et al.[13] that metals released in microniches
392 are removed by precipitation as their sulfides.

393 **Underlying mechanisms of small-scale mobilization of trace metals in two contrasting**
394 **sediments**. Mineralization of organic matter is the driving force of early diagenetic
395 transformations in marine sediments.[53,54] The mineralization process requires electron acceptors,
396 which are consumed until their depletion in the order oxygen, nitrate, iron and manganese oxy-

hydroxides, and sulfate, although sometimes the consumption can appear to occur concurrently.[23] When sulfate is also exhausted, organic matter can still be degraded via methanogenesis. In sediments of the BCZ of the North Sea substantial concentrations of Fe and Mn along with redox-sensitive cobalt occur in near surface sediments where microniche mobilization of Fe, Mn, and sulfide have previously been observed.[6,23] In the GB of the Baltic Sea, sediments are dominated by sulfide, but several microniches of elevated metals were observed, both in 1D profiles (Figures S5, S6, and S7) and 2D images (Figure 3). The observations are indicators of different diagenetic processes.

In BCZ sediment, sulfide is low, but present throughout the sediment profile with increased concentration immediately below the interface (Figure S4), indicating sulfate being used throughout as an electron acceptor. The elevated concentrations of dissolved Fe and Mn in near surface sediments shown in the 1D profiles, suggest their oxides are also electron acceptors. However, the high resolution 2D images suggest different process may be occurring. The more uniform Mn distribution is consistent with modeling studies[17,35] that indicated supply of Mn(II) from dissolution of carbonate minerals. As there is some correspondence between Mn and Co (Figure 4C, Table 1), indicative of some coupling through their established redox characteristics, the two processes appear to contribute to Mn mobilization.

In contrast to BCZ sediment, GB sediments are dominated by sulfide and completely anoxic (Figures S5, S6, and S7). The high concentrations of sulfide ensure low concentrations of Fe. If reactive organic matter, mainly consisting of phytoplankton aggregates,[55,56] are displaced from the surface before decomposition, their constituent trace metals are released, causing the observed localized maxima. The decomposition of this reactive organic matter is probably caused by methanogenesis:

$$2CH_2O + H_2O \rightarrow CH_4 + H^+ + HCO_3^-$$

Previous studies have demonstrated that in sulfate reducing zones, methanogenesis and sulfate reduction can be concurrently active, where members of the family *Methanosarcinaceae*[57,58] and *Desulfobacteraceae*[59] are responsible for the two processes.

Environmental implications. 2D-HR imaging of the mobilization of metals in sediments revealed two important features that cannot be fully inferred from 1D profiles, the clear horizontal mobilization gradients and the existence of localized microniches. Care should be exercised in attributing coincident maxima of metals in 1D profiles to mechanisms, as our 2D imaging of BCZ sediments showed that Fe and Co were not co-mobilized, even though they both had sub-surface 1D maxima. According to Ho et al.[60], the size of fragments of organic particles in sediments could be as small as 10 μm. As their decomposition drives metal mobilization, either through direct release or associated reductive or acidic dissolution processes, the mobilization of metals in sediment may be inherently discrete and take place at a very small scale. Traditional sampling where sediment is sliced and porewater extracted from at least tens of mL of sediment, automatically averages such features and therefore interpretations focus on the overall diagenetic reactions. The 1D DGT used here effectively samples ~0.1 mL of sediment for each data point. At this resolution microniches of mobilization will not be averaged, but they are ill defined. They therefore appear in the vertical profile as maxima of 1 or a few data points, making the profile look inherently noisy. It would be wrong to dismiss the localized microniches that are fully resolved by the 2D imaging as too small to have any importance. They can make a significant contribution to organic matter turnover and element cycling in aquatic sediments.[61,62] If microniches were to account for only 1% of the total available organic matter, but had turnover rates 50 times higher than the bulk material, the microniche activity would account for one third

443 of the carbon turnover of the whole system.[3] The prevalence of microniches was demonstrated by
444 Widerlund and Davison[14] recording over 3000 sulfide microniches in the sediments of an
445 eutrophic lake over a five-months period. Elevated trace metal mobilization was found in sulfidic
446 microniches in this lake and in marine sediments.[6,20] When sulfide is plentiful, as in the GB,
447 metal sulfide formation is responsible for the steep removal of metal away from the source.
448 Substantial release of trace metals from microniches to adjacent porewater can be expected if
449 sulfide concentrations are low, as observed by Lehto et al.[19] who found that metal microniches at
450 the SWI of a marine harbour sediment generated considerable effluxes of Fe, Mn, and Pb to the
451 water column.

452 Our novel approach allowed us to identify the prevalence of microniches of metal mobilization
453 using 1D profiles. More detailed 2D images were then able to geometrically define local
454 mobilization zones and charcterise coincident mobilization of various chemical compounds.
455 Those discoveries helped us to better understand the mobilization mechanisms of trace metals in
456 marine sediments in relation to the prevailing environmental conditions. For example, Co and Fe
457 mobilization were shown to be mutually exclusive, even though they were coincident in 1D
458 profiles. A well-defined local microniche of Co and Ni mobilization was shown to be supplied
459 from localized decomposition of reactive organic material rather than release from reductively
460 dissolving Fe or Mn oxides. However, there are limitations to 2D-HR imaging. It is clear that 1D
461 profiles are much easier to obtain than 2D images and provide information over often relevant
462 distances of tens of cm. Therefore, to assess potential mobilization zones it is recommended to
463 first obtain 1D profiles. However, traditional measurements based on sediment core slicing that
464 complement the DGT profiles and images should not be overlooked because (1) a wider range of
465 analytes, including a number that cannot be measured by DGT, can be assessed in this way; (2)

466 with DGT only labile trace metal concentrations in sediment porewater (free ions and easily
467 dissociated complexes) are measured,[63,64] while the total dissolved concentration is assessed by
468 the traditional method. Further progress is likely to come from combining such data and allying it
469 to kinetic and equilibrium data on the solid phase.[64]

ACKNOWLEDGEMENTS

C. Zhou is supported by Chinese Scholarship Council (PhD fellowship 201606190219). C. Gaulier and M. Luo are supported by NewSTHEPS project (BR/143/A2/NEWSTHEPS). The authors would like to thank the FWO research grant (1529016N) and Hercules Foundation (UABR/11/010) for LA-ICP-MS. The RV Belgica crew members, the scientific vessel of the Belgian government is thanked for the sampling campaigns. M. Leermakers is thanked for the sample analysis.

SUPPORTING INFORMATION

Materials and methods: additional information of sampling stations; hydrogen to sodium form conversion of the ground Chelex-100 resin; calibration of sulfide measurement by DGT; QA/QC. Results and Discussion: general features of the sediments in BCZ and GB; comparison of the horizontal distribution between sulfide and metals in zone 2; mineral saturation index calculation for metal sulfides inside and outside the microniche by Visual Minteq. Tables S1-4: the blank and detection limit of a ground Chelex-100 binding gel; optimized operating parameters of LA-ICP-MS; certified and measured concentrations of target elements in the SLRS-6 reference material; calculated saturation indices of metal sulfides inside and outside microniche. Figures S1-8: map of the sampling sites; the sulfide calibration curve measured by DGT; depth profiles of pH; 1D profiles of metals and sulfide in the sediments at station 130 (BCZ) and at stations 8, 6, and 14 (GB); horizontal distribution of the concentrations of metals and sulfide in zone 2.

REFERENCES

(1) Shaw, T. J.; Gieskes, J. M.; Jahnke, R. A. Early Diagenesis in Differing Depositional Environments: The Response of Transition Metals in Pore Water. *Geochim. Cosmochim. Acta* **1990**, *54* (5), 1233–1246. https://doi.org/10.1016/0016-7037(90)90149-F.

(2) Fones, G. R.; Davison, W.; Hamilton-Taylor, J. The Fine-Scale Remobilization of Metals in the Surface Sediment of the North-East Atlantic. *Cont. Shelf Res.* **2004**, *24* (13–14), 1485–1504. https://doi.org/10.1016/J.CSR.2004.05.007.

(3) Stockdale, A.; Davison, W.; Zhang, H. Micro-Scale Biogeochemical Heterogeneity in Sediments: A Review of Available Technology and Observed Evidence. *Earth-Science Rev.* **2009**, *92* (1–2), 81–97. https://doi.org/10.1016/j.earscirev.2008.11.003.

(4) Tankere-Muller, S.; Zhang, H.; Davison, W.; Finke, N.; Larsen, O.; Stahl, H.; Glud, R. N. Fine Scale Remobilisation of Fe, Mn, Co, Ni, Cu and Cd in Contaminated Marine Sediment. *Mar. Chem.* **2007**, *106* (1-2 SPEC. ISS.), 192–207. https://doi.org/10.1016/j.marchem.2006.04.005.

(5) Stahl, H.; Warnken, K. W.; Sochaczewski, L.; Glud, R. N.; Davison, W.; Zhang, H. A Combined Sensor for Simultaneous High Resolution 2-D Imaging of Oxygen and Trace Metals Fluxes. *Limnol. Oceanogr. Methods* **2012**, *10* (5), 389–401. https://doi.org/10.4319/lom.2012.10.389.

(6) Gao, Y.; van de Velde, S.; Williams, P. N.; Baeyens, W.; Zhang, H. Two-Dimensional Images of Dissolved Sulfide and Metals in Anoxic Sediments by a Novel Diffusive Gradients in Thin Film Probe and Optical Scanning Techniques. *TrAC - Trends Anal. Chem.* **2015**, *66*, 63–71. https://doi.org/10.1016/j.trac.2014.11.012.

(7) Luther, G. W.; Brendel, P. J.; Lewis, B. L.; Sundby, B.; Lefrançois, L.; Silverberg, N.; Nuzzio, D. B. Simultaneous Measurement of O2, Mn, Fe, I-, and S(-II) in Marine Pore Waters with a Solid-State Voltammetric Microelectrode. *Limnol. Oceanogr.* **1998**, *43* (2), 325–333. https://doi.org/10.4319/lo.1998.43.2.0325.

(8) Taillefert, M.; Luther III, G. W.; Nuzzio, D. B. The Application of Electrochemical Tools for In Situ Measurements in Aquatic Systems. *Electroanalysis* **2000**, *12* (6), 401–412. https://doi.org/10.1002/(sici)1521-4109(20000401)12:6<401::aid-elan401>3.3.co;2-l.

(9) Larsen, M.; Borisov, S. M.; Grunwald, B.; Klimant, I.; Glud, R. N. A Simple and Inexpensive High Resolution Color Ratiometric Planar Optode Imaging Approach: Application to Oxygen and PH Sensing. *Limnol. Oceanogr. Methods* **2011**, *9* (9), 348–360. https://doi.org/10.4319/lom.2011.9.348.

(10) Yin, D.-X.; Fang, W.; Guan, D.-X.; Williams, P. N.; Moreno-Jimenez, E.; Gao, Y.; Zhao, F.-J.; Ma, L. Q.; Zhang, H.; Luo, J. Localized Intensification of Arsenic Release within the Emergent Rice Rhizosphere. *Environ. Sci. Technol.* **2020**, *54* (6), 3138–3147. https://doi.org/10.1021/acs.est.9b04819.

(11) Davison, W.; Zhang, H. In Situ speciation Measurements of Trace Components in Natural Waters Using Thin-Film Gels. *Nature* **1994**, *367* (6463), 546–548.

(12) Santner, J.; Larsen, M.; Kreuzeder, A.; Glud, R. N. Two Decades of Chemical Imaging of Solutes in Sediments and Soils - a Review. *Anal. Chim. Acta* **2015**, *878*, 9–42. https://doi.org/10.1016/j.aca.2015.02.006.

(13) Stockdale, A.; Davison, W.; Zhang, H. Formation of Iron Sulfide at Faecal Pellets and Other Microniches within Suboxic Surface Sediment. *Geochim. Cosmochim. Acta* **2010**,

533 *74* (9), 2665–2676. https://doi.org/10.1016/J.GCA.2010.02.005.

534 (14) Widerlund, A.; Davison, W. Size and Density Distribution of Sulfide-Producing
535 Microniches in Lake Sediments. *Environ. Sci. Technol.* **2007**, *41* (23), 8044–8049.
536 https://doi.org/10.1021/es071510x.

537 (15) Watling, L. Small-Scale Features of Marine Sediments and Their Importance to the Study
538 of Deposit-Feeding. *Mar. Ecol. Prog. Ser.* **1988**, *47*, 135–144.
539 https://doi.org/10.3354/meps047135.

540 (16) Zhu, Q.; Aller, R. C.; Fan, Y. Two-Dimensional PH Distributions and Dynamics in
541 Bioturbated Marine Sediments. *Geochim. Cosmochim. Acta* **2006**, *70* (19), 4933–4949.
542 https://doi.org/10.1016/j.gca.2006.07.033.

543 (17) van de Velde, S.; Lesven, L.; Burdorf, L. D. W.; Hidalgo-Martinez, S.; Geelhoed, J. S.;
544 Van Rijswijk, P.; Gao, Y.; Meysman, F. J. R. The Impact of Electrogenic Sulfur Oxidation
545 on the Biogeochemistry of Coastal Sediments: A Field Study. *Geochim. Cosmochim. Acta*
546 **2016**, *194*, 211–232. https://doi.org/10.1016/j.gca.2016.08.038.

547 (18) Schippers, A.; Jørgensen, B. B. Biogeochemistry of Pyrite and Iron Sulfide Oxidation in
548 Marine Sediments. *Geochim. Cosmochim. Acta* **2002**, *66* (1), 85–92.
549 https://doi.org/10.1016/S0016-7037(01)00745-1.

550 (19) Lehto, N. J.; Larsen, M.; Zhang, H.; Glud, R. N.; Davison, W. A Mesocosm Study of
551 Oxygen and Trace Metal Dynamics in Sediment Microniches of Reactive Organic
552 Material. *Sci. Rep.* **2017**, *7* (1), 11369–11480. https://doi.org/10.1038/s41598-017-10179-
553 3.

554 (20) Motelica-Heino, M.; Naylor, C.; Zhang, H.; Davison, W. Simultaneous Release of Metals

555 and Sulfide in Lacustrine Sediment. *Environ. Sci. Technol.* **2003**, *37* (19), 4374–4381.
556 https://doi.org/10.1021/es030035+.

557 (21) Zhou, C.; van de Velde, S.; Baeyens, W.; Gao, Y. Comparison of Chelex Based Resins in
558 Diffusive Gradients in Thin-Film for High Resolution Assessment of Metals. *Talanta*
559 **2018**, *186*, 397–405. https://doi.org/10.1016/j.talanta.2018.04.085.

560 (22) Sochaczewski, Ł.; Stockdale, A.; Davison, W.; Tych, W.; Zhang, H. A Three-Dimensional
561 Reactive Transport Model for Sediments, Incorporating Microniches. *Environ. Chem.*
562 **2008**, *5* (3), 218–225. https://doi.org/10.1071/EN08006.

563 (23) Naylor, C.; Davison, W.; Motelica-Heino, M.; Van Den Berg, G. .; Van Der Heijdt, L. .
564 Simultaneous Release of Sulfide with Fe, Mn, Ni and Zn in Marine Harbour Sediment
565 Measured Using a Combined Metal/Sulfide DGT Probe. *Sci. Total Environ.* **2004**, *328* (1–
566 3), 275–286. https://doi.org/10.1016/J.SCITOTENV.2004.02.008.

567 (24) Morse, J. W.; Luther, G. W. Chemical Influences on Trace Metal-Sulfide Interactions in
568 Anoxic Sediments. *Geochim. Cosmochim. Acta* **1999**, *63* (19–20), 3373–3378.
569 https://doi.org/10.1016/S0016-7037(99)00258-6.

570 (25) Dellwig, O.; Leipe, T.; März, C.; Glockzin, M.; Pollehne, F.; Schnetger, B.; Yakushev, E.
571 V.; Böttcher, M. E.; Brumsack, H.-J. A New Particulate Mn–Fe–P-Shuttle at the
572 Redoxcline of Anoxic Basins. *Geochim. Cosmochim. Acta* **2010**, *74* (24), 7100–7115.
573 https://doi.org/10.1016/J.GCA.2010.09.017.

574 (26) Jilbert, T.; Slomp, C. P. Iron and Manganese Shuttles Control the Formation of Authigenic
575 Phosphorus Minerals in the Euxinic Basins of the Baltic Sea. *Geochim. Cosmochim. Acta*
576 **2013**, *107*, 155–169. https://doi.org/10.1016/j.gca.2013.01.005.

(27) Hermans, M.; Lenstra, W. K.; van Helmond, N. A. G. M.; Behrends, T.; Egger, M.; Séguret, M. J. M.; Gustafsson, E.; Gustafsson, B. G.; Slomp, C. P. Impact of Natural Re-Oxygenation on the Sediment Dynamics of Manganese, Iron and Phosphorus in a Euxinic Baltic Sea Basin. *Geochim. Cosmochim. Acta* **2019**, *246*, 174–196. https://doi.org/10.1016/J.GCA.2018.11.033.

(28) Rathnayake Kankanamge, N.; Bennett, W. W.; Teasdale, P. R.; Huang, J.; Welsh, D. T. Comparing in Situ Colorimetric DET and DGT Techniques with Ex Situ Core Slicing and Centrifugation for Measuring Ferrous Iron and Dissolved Sulfide in Coastal Sediment Pore Waters. *Chemosphere* **2017**, *188*, 119–129. https://doi.org/10.1016/j.chemosphere.2017.08.144.

(29) Gao, Y.; Lesven, L.; Gillan, D.; Sabbe, K.; Billon, G.; De Galan, S.; Elskens, M.; Baeyens, W.; Leermakers, M. Geochemical Behavior of Trace Elements in Sub-Tidal Marine Sediments of the Belgian Coast. *Mar. Chem.* **2009**, *117* (1–4), 88–96. https://doi.org/10.1016/j.marchem.2009.05.002.

(30) Leermakers, M.; Gao, Y.; Gabelle, C.; Lojen, S.; Ouddane, B.; Wartel, M.; Baeyens, W. Determination of High Resolution Pore Water Profiles of Trace Metals in Sediments of the Rupel River (Belgium) Using DET (Diffusive Equilibrium in Thin Films) and DGT (Diffusive Gradients in Thin Films) Techniques. *Water. Air. Soil Pollut.* **2005**, *166* (1–4), 265–286. https://doi.org/10.1007/s11270-005-6671-7.

(31) Luo, J.; Zhang, H.; Davison, W.; McLaren, R. G.; Clucas, L. M.; Ma, L. Q.; Wang, X. Localised Mobilisation of Metals, as Measured by Diffusive Gradients in Thin-Films, in Soil Historically Treated with Sewage Sludge. *Chemosphere* **2013**, *90* (2), 464–470. https://doi.org/10.1016/J.CHEMOSPHERE.2012.07.064.

(32) Stockdale, A.; Davison, W.; Zhang, H.; Hamilton-Taylor, J. The Association of Cobalt with Iron and Manganese (Oxyhydr)Oxides in Marine Sediment. *Aquat. Geochemistry* **2010**, *16* (4), 575–585. https://doi.org/10.1007/s10498-010-9092-1.

(33) Swanner, E. D.; Planavsky, N. J.; Lalonde, S. V.; Robbins, L. J.; Bekker, A.; Rouxel, O. J.; Saito, M. A.; Kappler, A.; Mojzsis, S. J.; Konhauser, K. O. Cobalt and Marine Redox Evolution. *Earth Planet. Sci. Lett.* **2014**, *390*, 253–263. https://doi.org/10.1016/j.epsl.2014.01.001.

(34) Murray, J. W.; Dillard, J. G. The Oxidation of Cobalt(II) Adsorbed on Manganese Dioxide. *Geochim. Cosmochim. Acta* **1979**, *43* (5), 781–787. https://doi.org/10.1016/0016-7037(79)90261-8.

(35) van de Velde, S.; Callebaut, I.; Gao, Y.; Meysman, F. J. R. Impact of Electrogenic Sulfur Oxidation on Trace Metal Cycling in a Coastal Sediment. *Chem. Geol.* **2017**, *452*, 9–23. https://doi.org/10.1016/J.CHEMGEO.2017.01.028.

(36) Vijayaraghavan, K.; Jegan, J.; Palanivelu, K.; Velan, M. Biosorption of Copper, Cobalt and Nickel by Marine Green Alga Ulva Reticulata in a Packed Column. *Chemosphere* **2005**, *60* (3), 419–426. https://doi.org/10.1016/j.chemosphere.2004.12.016.

(37) van de Velde, S. J.; Hylén, A.; Kononets, M.; Marzocchi, U.; Leermakers, M.; Choumiline, K.; Hall, P. O. J.; Meysman, F. J. R. Elevated Sedimentary Removal of Fe, Mn, and Trace Elements Following a Transient Oxygenation Event in the Eastern Gotland Basin, Central Baltic Sea. *Geochim. Cosmochim. Acta* **2020**, *271*, 16–32. https://doi.org/10.1016/J.GCA.2019.11.034.

(38) Tribovillard, N.; Algeo, T. J.; Lyons, T.; Riboulleau, A. Trace Metals as Paleoredox and

622 Paleoproductivity Proxies: An Update. *Chem. Geol.* **2006**, *232* (1–2), 12–32.
623 https://doi.org/10.1016/j.chemgeo.2006.02.012.

624 (39) Böning, P.; Shaw, T.; Pahnke, K.; Brumsack, H. J. Nickel as Indicator of Fresh Organic
625 Matter in Upwelling Sediments. *Geochim. Cosmochim. Acta* **2015**, *162* (1), 99–108.
626 https://doi.org/10.1016/j.gca.2015.04.027.

627 (40) Tessier, A.; Fortin, D.; Belzile, N.; DeVitre, R. R.; Leppard, G. G. Metal Sorption to
628 Diagenetic Iron and Manganese Oxyhydroxides and Associated Organic Matter:
629 Narrowing the Gap between Field and Laboratory Measurements. *Geochim. Cosmochim.*
630 *Acta* **1996**, *60* (3), 387–404. https://doi.org/10.1016/0016-7037(95)00413-0.

631 (41) Belzile, N.; De Vitre, R. R.; Tessier, A. In Situ Collection of Diagenetic Iron and
632 Manganese Oxyhydroxides from Natural Sediments. *Nature* **1989**, *340*, 376–377.
633 https://doi.org/10.1038/340376a0.

634 (42) Norman, M. D.; De Deckker, P. Trace Metals in Lacustrine and Marine Sediments: A Case
635 Study from the Gulf of Carpentaria, Northern Australia. *Chem. Geol.* **1990**, *82*, 299–318.
636 https://doi.org/10.1016/0009-2541(90)90087-N.

637 (43) Douglas, G. B.; Adeney, J. A. Diagenetic Cycling of Trace Elements in the Bottom
638 Sediments of the Swan River Estuary, Western Australia. *Appl. Geochemistry* **2000**, *15*
639 (5), 551–566. https://doi.org/10.1016/S0883-2927(99)00070-0.

640 (44) Hamilton-Taylor, J.; Smith, E. J.; Davison, W.; Sugiyama, M. Resolving and Modeling the
641 Effects of Fe and Mn Redox Cycling on Trace Metal Behavior in a Seasonally Anoxic
642 Lake. *Geochim. Cosmochim. Acta* **2005**, *69* (8), 1947–1960.
643 https://doi.org/10.1016/J.GCA.2004.11.006.

644 (45) Span, D.; Gaillard, J. F. An Investigation of a Procedure for Determining Carbonate-
645 Bound Trace Metals. *Chem. Geol.* **1986**, *56* (1–2), 135–141. https://doi.org/10.1016/0009-
646 2541(86)90116-6.

647 (46) Tessier, A.; Campbell, P. G. C. Partitioning of Trace Metals in Sediments: Relationships
648 with Bioavailability. *Hydrobiologia* **1987**, *149*, 43–52.
649 https://doi.org/10.1007/BF00048645.

650 (47) Ho, T. Y.; Quigg, A.; Finkel, Z. V.; Milligan, A. J.; Wyman, K.; Falkowski, P. G.; Morel,
651 F. M. M. The Elemental Composition of Some Marine Phytoplankton. *J. Phycol.* **2003**, *39*
652 (6), 1145–1159. https://doi.org/10.1111/j.0022-3646.2003.03-090.x.

653 (48) Finkel, Z. V; Quigg, A.; Raven, J. A.; Reinfelder, J. R.; Schofield, O. E.; Falkowski, P. G.
654 Irradiance and the Elemental Stoichiometry of Marine Phytoplankton. *Limnol. Ocean.*
655 **2006**, *51* (6), 2690–2701.

656 (49) Suikkanen, S.; Laamanen, M.; Huttunen, M. Long-Term Changes in Summer
657 Phytoplankton Communities of the Open Northern Baltic Sea. *Estuar. Coast. Shelf Sci.*
658 **2007**, *71* (3–4), 580–592. https://doi.org/10.1016/J.ECSS.2006.09.004.

659 (50) Carman, R.; Rahm, L. Early Diagenesis and Chemical Characteristics of Interstitial Water
660 and Sediments in the Deep Deposition Bottoms of the Baltic Proper. *J. Sea Res.* **1997**, *37*
661 (1–2), 25–47. https://doi.org/10.1016/S1385-1101(96)00003-2.

662 (51) Lukawska-Matuszewska, K. Contribution of Non-Carbonate Inorganic and Organic
663 Alkalinity to Total Measured Alkalinity in Pore Waters in Marine Sediments (Gulf of
664 Gdansk, S-E Baltic Sea). *Mar. Chem.* **2016**, *186* (20), 211–220.
665 https://doi.org/10.1016/j.marchem.2016.10.002.

(52) Ingri, J.; Widerlund, A.; Suteerasak, T.; Bauer, S.; Elming, S.-Å. Changes in Trace Metal Sedimentation during Freshening of a Coastal Basin. *Mar. Chem.* **2014**, *167*, 2–12. https://doi.org/10.1016/J.MARCHEM.2014.06.010.

(53) Burdige, D. J. Estuarine and Coastal Sediments - Coupled Biogeochemical Cycling. In *Treatise on Estuarine and Coastal Science*; Elsevier Inc., 2012; Vol. 5, pp 279–316. https://doi.org/10.1016/B978-0-12-374711-2.00511-8.

(54) Emerson, S.; Hedges, J. Sediment Diagenesis and Benthic Flux. In *The oceans and Marine Geochemistry*; Elderfield, H., Ed.; Elsevier Ltd., 2006; pp 293–319.

(55) Nilsson, M. M.; Kononets, M.; Ekeroth, N.; Viktorsson, L.; Hylén, A.; Sommer, S.; Pfannkuche, O.; Almroth-Rosell, E.; Atamanchuk, D.; Andersson, J. H.; Roos, P.; Tengberg, A.; Hall, P. O. J. Organic Carbon Recycling in Baltic Sea Sediments – An Integrated Estimate on the System Scale Based on in Situ Measurements. *Mar. Chem.* **2019**, *209*, 81–93. https://doi.org/10.1016/j.marchem.2018.11.004.

(56) Walve, J.; Gelting, J.; Ingri, J. Trace Metals and Nutrients in Baltic Sea Cyanobacteria: Internal and External Fractions and Potential Use in Nitrogen Fixation. *Mar. Chem.* **2014**, *158*, 27–38. https://doi.org/10.1016/j.marchem.2013.11.002.

(57) Whiticar, M. J. Diagenetic Relationships of Methanogenesis, Nutrients, Acoustic Turbidity, Pockmarks and Freshwater Seepages in Eckernförde Bay. *Mar. Geol.* **2002**, *182* (1–2), 29–53. https://doi.org/10.1016/S0025-3227(01)00227-4.

(58) Treude, T.; Krüger, M.; Boetius, A.; Jørgensen, B. B. Environmental Control on Anaerobic Oxidation of Methane in the Gassy Sediments of Eckernförde Bay (German Baltic). *Limnol. Oceanogr.* **2005**, *50* (6), 1771–1786. https://doi.org/10.4319/lo.2005.50.6.1771.

(59) Edlund, A.; Hårdeman, F.; Jansson, J. K.; Sjöling, S. Active Bacterial Community Structure along Vertical Redox Gradients in Baltic Sea Sediment. *Environ. Microbiol.* **2008**, *10* (8), 2051–2063. https://doi.org/10.1111/j.1462-2920.2008.01624.x.

(60) Ho, T. Y.; Wen, L. S.; You, C. F.; Lee, D. C. The Trace-Metal Composition of Size-Fractionated Plankton in the South China Sea: Biotic versus Abiotic Sources. *Limnol. Oceanogr.* **2007**, *52* (5), 1776–1788. https://doi.org/10.4319/lo.2007.52.5.1776.

(61) Glud, R. N.; Stahl, H.; Berg, P.; Wenzhöfer, F.; Oguri, K.; Kitazato, H. In Situ Microscale Variation in Distribution and Consumption of O2: A Case Study from a Deep Ocean Margin Sediment (Sagami Bay, Japan). *Limnol. Oceanogr.* **2009**, *54* (1), 1–12. https://doi.org/10.4319/lo.2009.54.1.0001.

(62) Lehto, N.; Glud, R. N.; á Nordi, G.; Zhang, H.; Davison, W. Anoxic Microniches in Marine Sediments Induced by Aggregate Settlement: Biogeochemical Dynamics and Implications. *Biogeochemistry* **2014**, *119*, 307–327. https://doi.org/10.1007/s10533-014-9967-0.

(63) Gao, Y.; Zhou, C.; Gaulier, C.; Bratkic, A.; Galceran, J.; Puy, J.; Zhang, H.; Leermakers, M.; Baeyens, W. Labile Trace Metal Concentration Measurements in Marine Environments: From Coastal to Open Ocean Areas. *TrAC Trends Anal. Chem.* **2019**, *116*, 92–101. https://doi.org/10.1016/J.TRAC.2019.04.027.

(64) Zhang, H.; Lombi, E.; Smolders, E.; McGrath, S. Kinetics of Zn Release in Soils and Prediction of Zn Concentration in Plants Using Diffusive Gradients in Thin Films. *Environ. Sci. Technol.* **2004**, *38* (13), 3608–3613. https://doi.org/10.1021/es0352597.

710

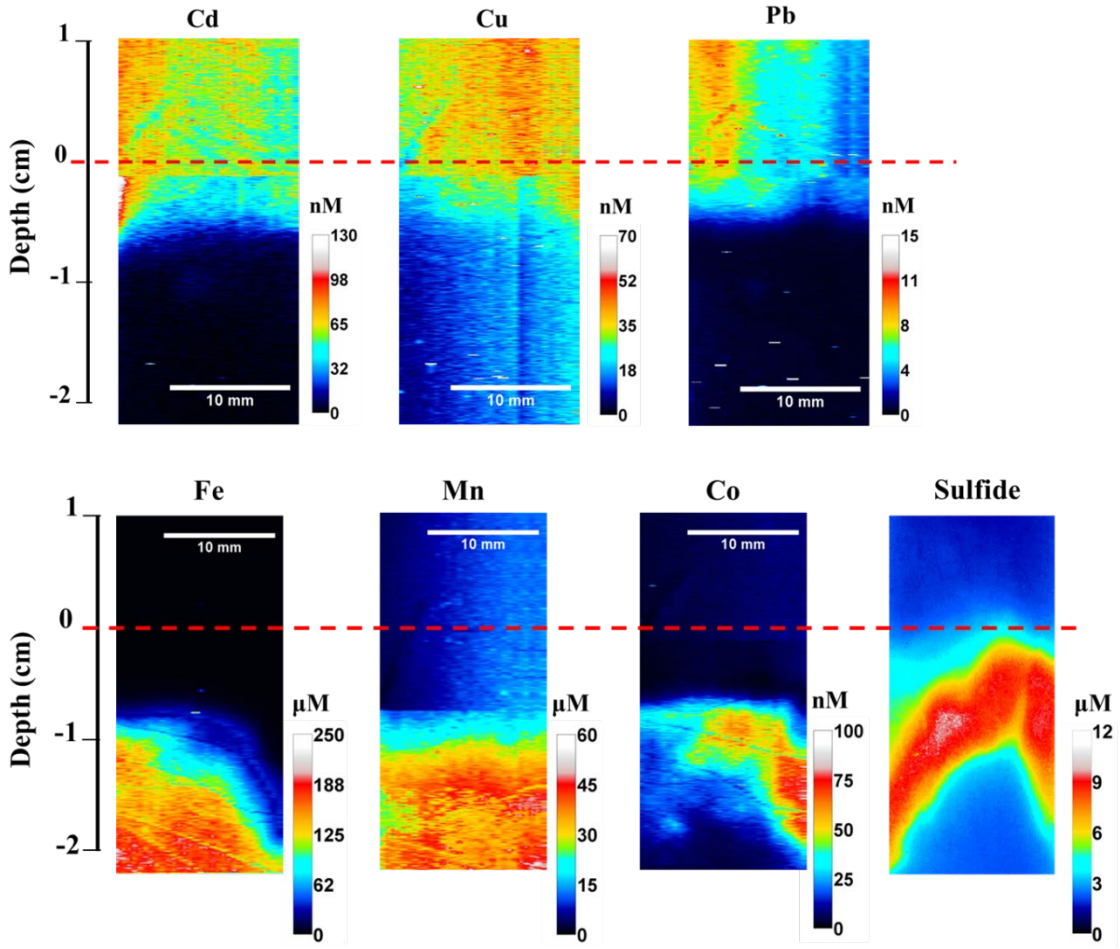

711

712 Figure 1. Two dimensional, high-resolution (2D-HR) images of dissolved metals and dissolved

713 sulfide at the sediment-water interface (SWI, 1 to -2 cm depth) of station 130 (BCZ).

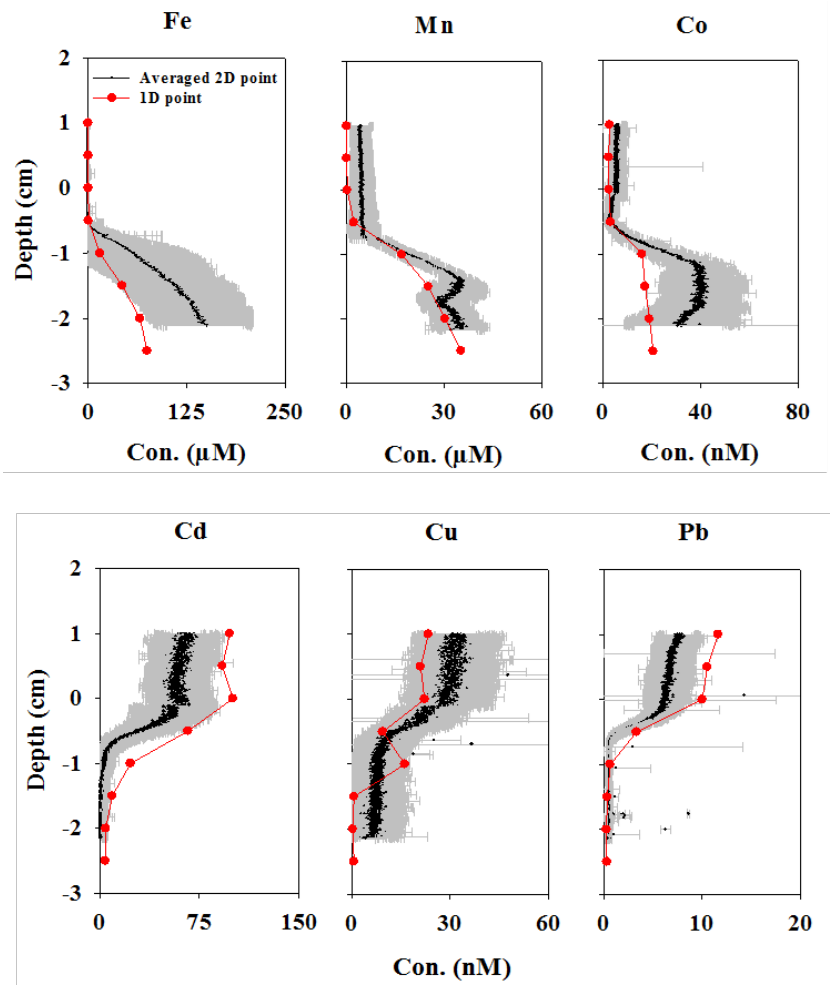

Figure 2. Comparison of the vertical profiles of metals at the SWI (1 to -2 cm depth) of station 130 between 1D profiles (red points, collected from Figure S4) and horizontally averaged 2D images (black points with the grey bars representing the standard deviations, collected from Figure 1).

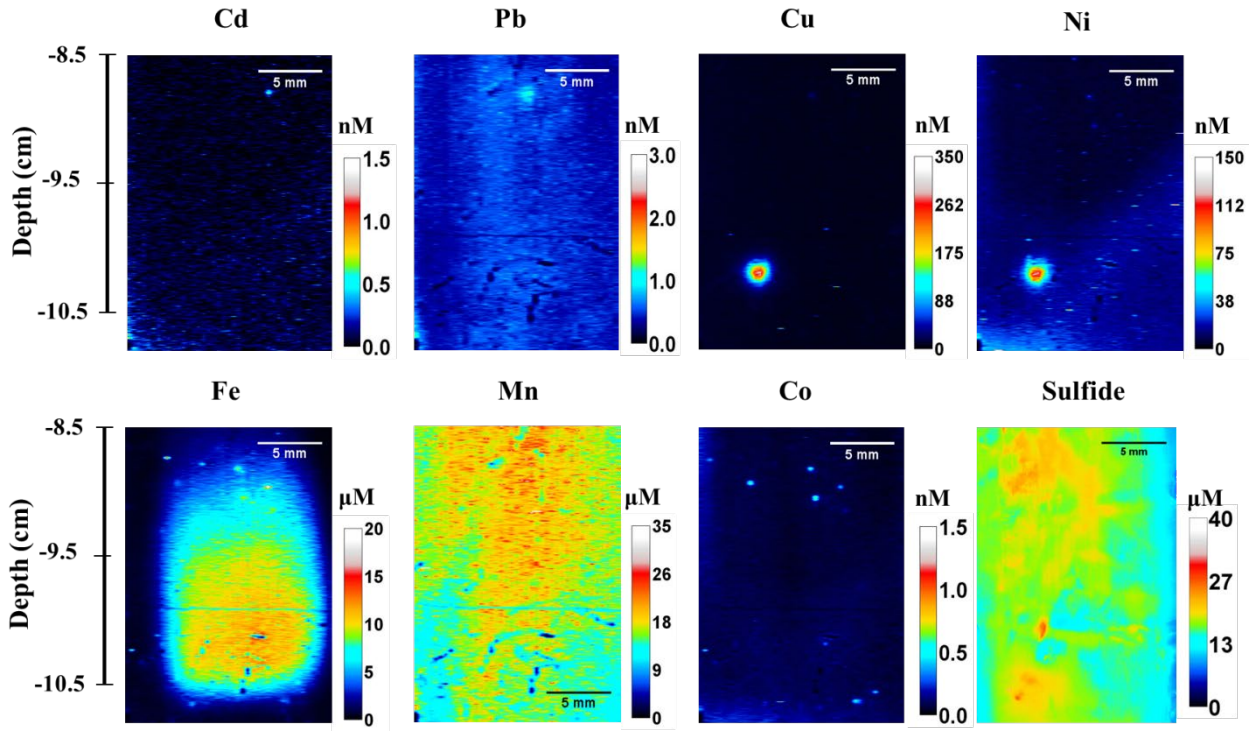

721

722 Figure 3. Two dimensional, high resolution (2D-HR) images of dissolved metals and dissolved

723 sulfide in sub-surface sediment (-8.5 to -10.5 cm depth) at station 16 (GB).

724

725

726

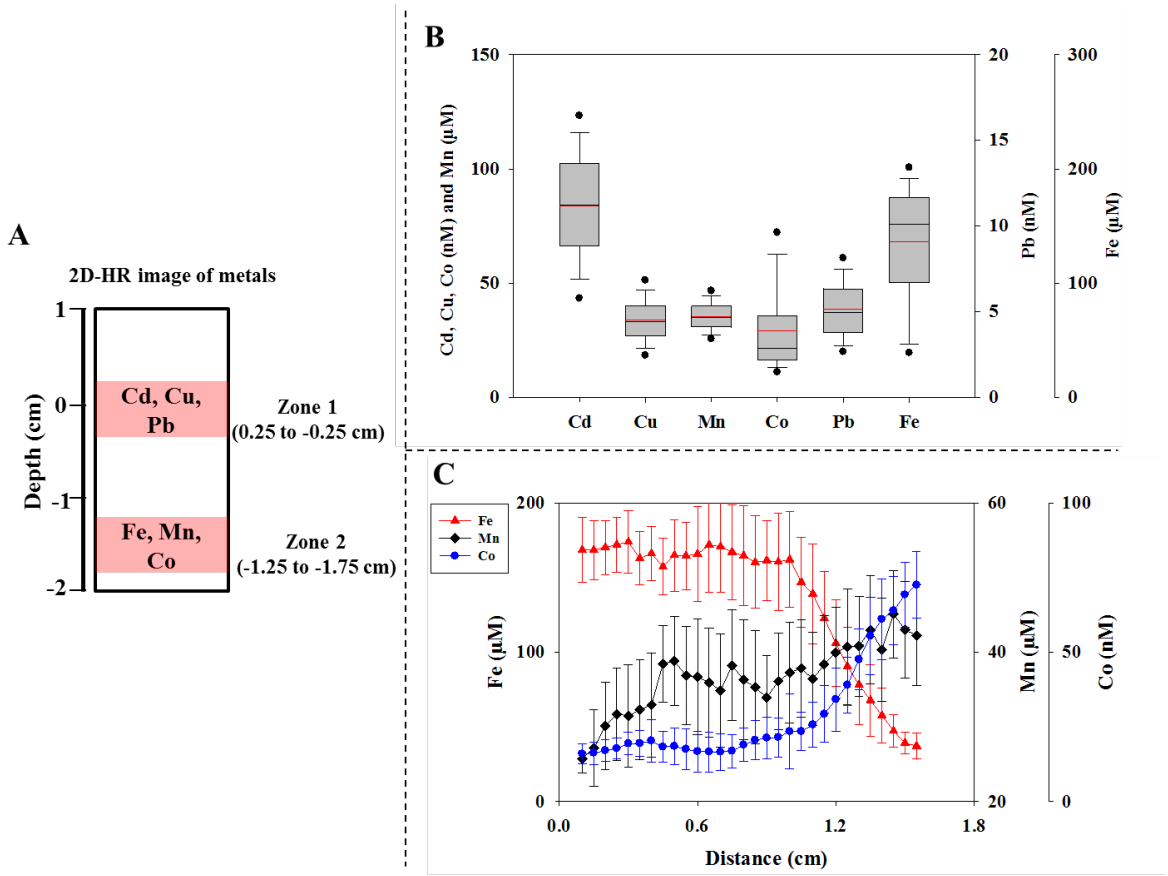

727

728 Figure 4. (A) shows two selected zones in the 2D-HR image of metals in the sediment at BCZ
729 station 130 (2D-HR results are shown in Figure 1). Each selected zone corresponds to a single
730 concentration point in the 1D profile at station 130 (1D results are shown in Figures 2 and S4).
731 Concentration values of Cd, Cu, and Pb were selected from zone 1 (0.25 to -0.25 cm of depth)
732 corresponding to the 1D result at 0 cm of depth, while those of Fe, Mn, and Co were selected
733 from zone 2 (-1.25 to -1.75 cm of depth) corresponding to the 1D result at -1.5 cm of depth. (B)
734 is the box plot showing the range and distribution of the concentration values of metals in the
735 selected zones in the 2D-HR image. Each grey box includes values between 25th and 75th
736 percentile with the black line inside indicating the median value and the red line inside indicating
737 the mean value. The whiskers above and below the box show the maximum (75th percentile + 1.5
738 × interquartile range) and minimum (25^{th} percentile – 1.5 × interquartile range) values. Two

739 points at the bottom and top represent 5th and 95th percentile respectively. (C) shows the
740 horizontal distribution of the concentrations of Fe, Mn, and Co in zone 2. The horizontal axis
741 presents the distance from the left edge, set at 0 cm.

742

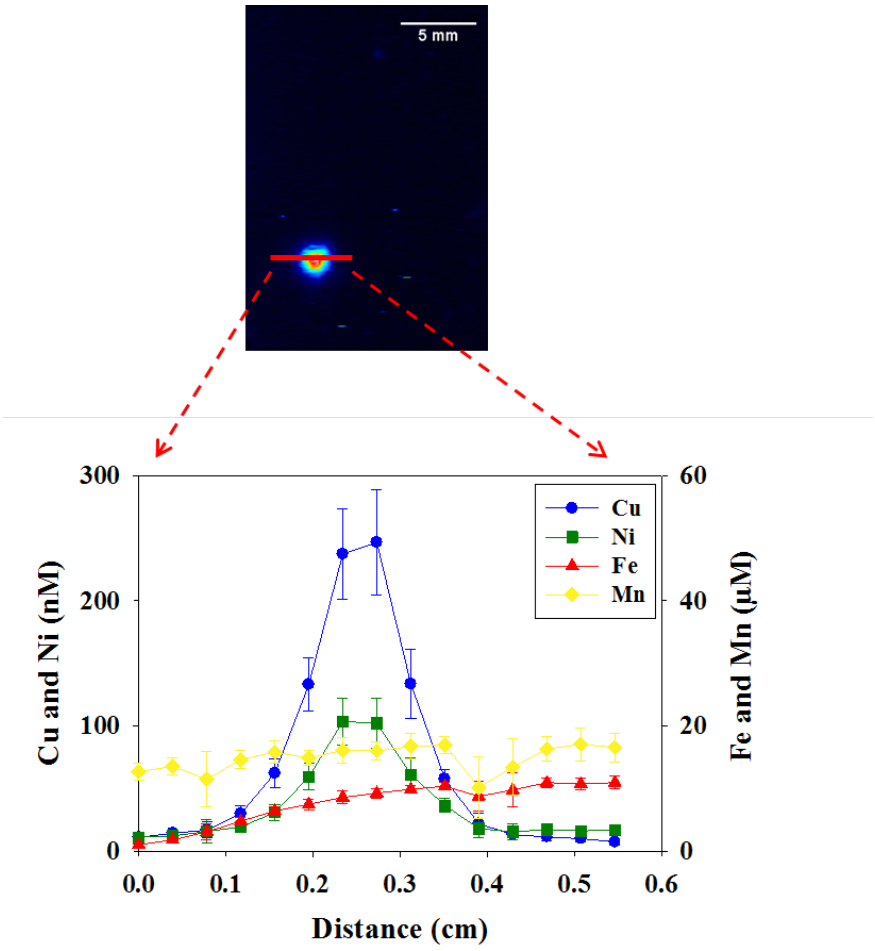

743

744 Figure 5. The concentration distribution of metals (Fe, Mn, Cu, and Ni) along the red line across

745 the observed microniche in the sediment at station 16 (GB).

746